



## Research Paper

## The Clay-SRB (sulfate-reducing bacteria) system: Dissolution and fractionation of REY



Simiao Li<sup>a</sup>, Yuntao Jing<sup>a,b</sup>, Xiangyu Zhu<sup>c</sup>, Yan Liu<sup>b</sup>, Hui Henry Teng<sup>c</sup>, Hongxia Du<sup>d</sup>, Wanfu Zhao<sup>e</sup>, Ming Ma<sup>d</sup>, Junfeng Ji<sup>f</sup>, Wancang Zhao<sup>a,\*</sup>

<sup>a</sup> Chongqing Key Laboratory of Karst Environment, School of Geographical Sciences, Southwest University, Chongqing 400715, PR China

<sup>b</sup> Institute of Geology, Chinese Academy of Geological Sciences, Beijing 100037, PR China

<sup>c</sup> School of Earth System Science, Tianjin University, Tianjin 300072, PR China

<sup>d</sup> College of Resources and Environment, Southwest University, Chongqing 400715, PR China

<sup>e</sup> Ningxia Institute of Land Resources Survey and Monitor, Yinchuan 750002, PR China

<sup>f</sup> Key Laboratory of Surficial Geochemistry, Ministry of Education, School of Earth Sciences and Engineering, Nanjing University, Nanjing 210093, PR China

## ARTICLE INFO

## Keywords:

Clay-sized minerals  
Sulfate-reducing bacteria (SRB)  
Bio-leaching  
Ion-adsorption REY deposits

## ABSTRACT

Rare earth elements (REYs) originate from the weathering of parent granite, whose clay-sized fractions are pivotal in the regolith-hosted rare earth elements (REEs) deposits. Regarding microbial action on REY mobilization and fractionation, their patterns remain unclear. Chemical extraction and bio-leaching experiments utilizing sulfate-reducing bacteria (SRB) were performed to exemplify the chemical and microbial effects on REY mobilization among the clay-sized phases. Our results indicate that the REYs occur primarily in the three fractions: i.e., amorphous Fe–Mn phase, crystalline Fe phase, and carbonate in chemical reactors wherein the mineral phase was critical to the adsorption of REY. The 30-day SRB-leaching experiments led to an increase in the percentage of REY from 6% to 45% in the residue phase, implying that the residue phase, R<sub>Amor</sub> iron phase, and R<sub>org</sub> phase hosted the REYs. The disorder of iron-bearing minerals, formation of iron-organic matters (Fe-OM), and secondary iron-bearing minerals represented a significant bio-leaching mechanism. Compared to chemical extraction, relatively higher MREY and HREY release efficiencies were obtained via bio-leaching, with average LREY/HREY ratios of 1.34–5.91 and 0.2–2.24 in chemical and bio-reactors, respectively. Our findings exhibited high potential microbial effects on the mobilization and fractionation of REY among mineral phases, offering real insights into the biogeochemical processes between minerals and bacteria.

## 1. Introduction

Rare earth elements (REY, lanthanides plus Y and Sc) are widely utilized for aerospace, military, new energy, electronic, and industrial applications (Xiao et al., 2015; Xu et al., 2017). The heavy rare earth elements (HREYs) are in particular demand for cutting-edge technology (Li et al., 2019). Global consumption of REYs has been increasing in recent years. Currently, ion-adsorption REE deposits in South China are crucial REY sources, supplying >95% of global HREY demand (Zhou et al., 2019; Wang et al., 2023).

The traditional extraction approach for ion-adsorption REY deposits encompasses in situ leaching according to the ion-exchange mechanism (Ou et al., 2022), capable of retrieving 80–90% of the total REY (Moldoveanu and Papangelakis, 2013). However, the outflow of ammonium

in the leaching process and excess ammonium residue in tailings cause severe pollution (Liu et al., 2019; Zhang et al., 2020; Liu et al., 2021a). Sequential chemical extraction is a typical laboratory approach, often utilized to quantitatively characterize and chemically isolate individual mineral phases (Poulton and Canfield, 2005). Recently, sequential leaching experiments on regolith samples have demonstrated that a large amount of REY could be extracted, and REYs intend to be absorbed by clay minerals (Bao and Zhao, 2008; Li and Zhou, 2020). Clay-sized sediments (< 2 μm) are the main component of the regolith in ion-adsorption deposits (accounting for about 45%) and are also the main occurrences of REYs in regolith (Li and Zhou, 2020). REYs in the clay-sized fractions are mainly absorbed by clay minerals (especially halloysite and kaolinite, Li et al., 2019) through ion exchange and surface complexation, followed by iron (hydroxide)oxides. However, few

\* Corresponding author.

E-mail address: [wancangzhao@nju.edu.cn](mailto:wancangzhao@nju.edu.cn) (W. Zhao).

studies have quantified the REY hosting in clay-sized sediments (< 2  $\mu\text{m}$ ).

Important progress has been made in the application of green nanotechnology and advanced materials such as magnetically retrievable  $\text{CoFe}_2\text{O}_4@\text{SiO}_2@\text{Dy}_2\text{Ce}_2\text{O}_7$  nanocomposites, rod-like  $[\text{Cu}(\text{phen})_2(\text{OAc})]\text{PF}_6$  complex, direct Z-scheme heterojunction photocatalyst, and zirconium dioxide ( $\text{ZrO}_2$ ) nanostructures (Zinatloo-Ajabshir and Salavati-Niasari, 2016; Zinatloo-Ajabshir and Salavati-Niasari, 2019; Hosseinzadeh et al., 2023; Zinatloo-Ajabshir et al., 2024), which have environmental and economic benefits. Besides the new nanotechnology and materials, increasing experimental studies indicated that bacteria had a high potential for mining and reducing ecological pollution (Li et al., 2022; Yan et al., 2023; He et al., 2023). Bioleaching is technologically feasible for REY extraction, and thus, many improvements of this biotechnology are required to modernize the mining industry and enhance the economic profit of REY extraction (Owusu-Fordjour and Yang, 2023). Microbes, as nonnegligible weathering driving forces, can accelerate the dissolution of REY-bearing minerals (Fathollahzadeh et al., 2018; He et al., 2023). However, the efficiency and preference for REY extraction are unclear, with few studies focused on the changes in the composition and morphology of clay-sized minerals (e.g., iron oxides and clay minerals) before and after the introduction of bacteria, the main host for REY may weather from the parent rock (Li and Zhou, 2020; Huang et al., 2021), to understand the microbial extracting of REYs in ion-adsorption deposits.

In the area of regolith-hosted rare earth elements (REE) deposits, sulfate-reducing bacteria (SRB) are found in abundance in the regolith (Yan et al., 2023). Given that the redox environment impacts the release of rare earth elements (Xiao et al., 2024), sulfate-reducing bacteria (SRB) can utilize organic matter as a carbon source and electron donor to transform  $\text{SC}_4^{2-}$  as the terminal electron acceptor into various sulfide forms ( $\text{H}_2\text{S}$ ,  $\text{HS}^-$ ,  $\text{S}^{2-}$ ) as respiratory products (Ko et al., 2017; Kumar et al., 2021; Li et al., 2024). Moreover, according to Gu et al. (2019), SRB consumes elemental iron as an electron donor when lacking low-molecular-weight organic compounds (carbon sources). Compared to other microbes (e.g., *Bacillus velezensis*, *Paenibacillus alvei*, and *Burkholderia fungorum*), which could accelerate the dissolution of granite and granite-forming minerals and have effects on the mobilization and distribution of REY during granite weathering (Taunton et al., 2000; Wu et al., 2008; He et al., 2023), SRB prefer reacting with clay-sized minerals, or even with REYs to accelerate the dissolution of REY. As a viable solution, bioleaching via SRB is positioned to address REY behaviors by a clay-SRB-REY redox system.

The primary goal of this study is to examine the microbial effects on the mobilization and fractionation of the clay-sized REY and make a comparison with the chemical effects. The REY-rich samples were collected from the Hanfang regolith-hosted deposit in the southern portion of Jiangxi Province, China. Leaching experiments under biotic and abiotic conditions were conducted to address the dissolution and fractionation of REY during the extraction process. Our results uncovered the microbial effects on REY dissolution and fractionation during the bio-reactions and found that the bio-leaching approach had a high potential for REY extraction.

## 2. Materials and Methods

### 2.1. Sample preparation and extraction of clay-size fractions from samples

Four soil samples, ZK01, ZK34, ZK81, and ZK105, were obtained from the Hanfang regolith-hosted REE deposit, in Ganzhou, Jiangxi Province, Southeast China (Li et al., 2017; He et al., 2023). They were processed to extract the clay-sized fractions separated from bulk samples through centrifugation in deionized water according to Stokes law, following the method optimized by Ji et al. (1999) and Zhao et al. (2015).

### 2.2. Sequential chemical extraction

The sequential chemical extraction procedure followed the method of Lu et al. (2017), which was modified from Poulton and Canfield (2005). In this study, approximately four REY-rich clay-sized samples of 100 mg each were weighed, and six steps were performed to extract various mineral phases and analyze the content of REY in each mineral phase.

We first removed the organic matter (step 1) followed by the carbonate (step 2) in the samples using 30%  $\text{H}_2\text{O}_2$  and 1 M acetic acid, respectively. After steps 1 and 2, a combination of 37.5 mL of 1 M hydroxylamine hydrochloride and 12.5 mL acetic acid was applied to extract the amorphous iron phase (easily reducible Fe oxides;  $\text{Fe}_{\text{ox1}}$ ; e.g., ferrihydrite and lepidocrocite, Poulton and Canfield, 2005) from the carbonate and organic free clay fraction of the samples. Following complete mixing, the samples were placed in the dark. Following step 3, the precipitate reacted with a mixture of CBD (45 mL of 0.3 M citrate, 5 mL of 1 M bicarbonate solution, and excess dithionite powder) to dissolve the crystalline iron phase (reducible Fe oxides;  $\text{Fe}_{\text{ox2}}$ ; e.g., hematite and goethite; Mehra and Jackson, 1958). The samples were heated in a water bath until the color of the residues changed from brown to green-grey. The phyllosilicate phase ( $\text{Fe}_{\text{HCl}}$ ; e.g., kaolinite and chlorite; Poulton and Canfield, 2005) was extracted through boiling with 3 mL of 6 M HCl. After boiling for 2 h, the color of the residues changed from green-grey to white. The volume was adjusted to 10 mL with purified water. The residual Fe phase ( $\text{Fe}_R$ ; e.g., illite) was digested using a mixture of aqua regia and hydrofluoric acid (HF). The residual samples were combined with 4 mL aqua regia and heated at 130 °C for 2 h until evaporated. Then, the residual phase was dissolved in 1 mL HF until completely dissolved. The volume was adjusted to 15 mL by the addition of 0.1 M  $\text{HNO}_3$ .

After every extraction step, the samples and reagent were centrifuged for 15 min at 4200 rpm and the levels of REY were measured in the diluted supernatant by inductively coupled plasma mass spectrometry (ICP-MS, Agilent 7900). The elemental contents in each dissolved phase concerning clay-sized sediment composition were calculated by the contents in each extracted solution multiplied by the volume of added solution and divided by the initial mass of clay-sized sediment. The concentration of major and trace elements in the chemically extracted fraction was measured by an inductively coupled plasma optical emission spectrometry (ICP-OES, Perkin-Elmer OPTIMA 8300) and a quadrupole ICP-MS, respectively. Analytical uncertainties were below 5%.

### 2.3. Bio-extracting experiments

#### 2.3.1. Removing of mineral phases

Approximately 500 mg of the clay-sized fractions were used for sequential chemical extraction again to remove various mineral phases. Details for procedures of mineral phase removal are presented in Text S1. Six kinds of residual clay phases were obtained after the 6-step reaction (clay fraction,  $\text{R}_{\text{Org}}$ ,  $\text{R}_{\text{Car}}$ ,  $\text{R}_{\text{Amor iron}}$ ,  $\text{R}_{\text{Cry iron}}$ , and residue phases).

#### 2.3.2. Culture of strain

SRB was isolated and purified from bulk purple paddy soil according to the method described by Li et al. (2022). DNA homology comparison was conducted to confirm the identity of the strain (Li et al., 2022; Yan et al., 2023). The SRB was cultured in a modified Postgate liquid medium (Postgate and Campbell, 1966) until reaching the log phase, resulting in the SRB fluid. The Postgate liquid medium was composed of 2.0 g/L  $\text{NaCl}$ , 1.0 g/L  $\text{NH}_4\text{Cl}$ , 2.0 g/L  $\text{MgSO}_4 \cdot 7\text{H}_2\text{O}$ , 0.5 g/L  $\text{Na}_2\text{SO}_4$ , 0.25 g/L  $\text{K}_2\text{HPO}_4$ , 5 mL/L 70% sodium lactate, 1.0 g/L yeast extract, 0.1 g/L ascorbic acid and 0.5 g/L L-cysteine, and the pH of the medium was adjusted to 7.0. To guarantee sterility, ascorbic acid and L-cysteine were sterilized using ultraviolet light for 30 min and added to the autoclaved medium.

### 2.3.3. The reaction system of SRB with the clay-sized fraction

To the initial reaction conditions of the SRB-clay model system, 200 mg of each above-mentioned clay-size mineral phase was included and sterilized by an autoclave at 120 °C for 20 min, which had little influence on the component and activity of organic matter. The SRB fluid was inoculated at a volume ratio of 1:25 (v/v), and the reaction system was maintained in a climate chamber at 35 °C for five days. The SRB solution was reconstituted every five days and inoculated. The incubation period was a total of 30 days. Thereafter, the resulting pellets were centrifuged and dried in an oven at 60 °C, and the REY contents were measured in the supernatant using a Thermo Fisher ICP-MS X2. The elemental contents in each reacted phase with respect to clay-sized sample composition were calculated by the contents in each extracted solution multiply by the volume of added solution and divided by the initial mass of the clay-sized sample.

### 2.4. Sample analyses

The XRD patterns of the harvested clay fractions were examined using the JADE 6.5 software package (MDI, USA). ATR-FTIR patterns were analyzed using Omnic 8.2 and Raman patterns were analyzed with Labspec 5.

Oriented section analysis was based on clay-sized fractions separated from bulk soil samples. Each oriented section was analyzed using a Bruker D8 Advance (German). These oriented sections were scanned with a goniometer from 3° to 50°, 20 stepped by 0.01° (Moore and Reynolds, 1997). The other following experimental parameters were used: soller slit = 4.1°/2.5°; divergence slit = 0.5° and anti-scatter slits = 5.1 mm. The detailed procedure was described by Lu et al. (2017) and Zhao et al. (2018). According to the positions of the (001) series of basal reflections on the XRD power diagrams, primary clay mineral compositions (i.e., kaolinite and illite) were identified by the air-dried curve constructed by the XRD diagram.

ATR-FTIR and Raman spectra (Key Laboratory of Surficial Geochemistry, Ministry of Education, Nanjing University) of functional group alterations in clay-size fractions, R<sub>Org</sub>, R<sub>Car</sub>, R<sub>Amor</sub> iron, R<sub>Cry</sub> iron, and residue phases with and without the addition of SRB were recorded using a Nicolet i50 FTIR spectrometer equipped with a diamond-tipped Attenuated Total Reflectance (ATR) device and a Raman spectrometer (LabRAM HR Evolution, HORIBA). The ATR-FTIR spectra of all samples correspond to 32 scans with resolutions of 4 cm<sup>-1</sup> and the wavenumber range was set as 4000–400 cm<sup>-1</sup>. When the sample was scanned, the room temperature was kept at 21 °C. The Raman spectra were obtained with a 50× objective; their accumulation, at a resolution of 2 cm<sup>-1</sup>, required 88 s. Before the Raman analysis, organic matter was removed using 30% H<sub>2</sub>O<sub>2</sub> to reduce interference. The samples were then heated in a water bath until no bubbles emerged.

Diffuse reflectance spectroscopy (DRS) analysis (Key Laboratory of Surficial Geochemistry, Ministry of Education, Nanjing University) was to characterize the changes of iron minerals in the clay system and SRB-clay system. Reflectance was measured using a Lambda 900 diffuse reflectance spectrometer, which scanned wavelengths from 400 to 1800 nm at 2 nm intervals. During measurements, a whiteboard composed of barium sulfate served as the background and standard of 100% lightness (Ji et al., 2002).

The minerals in the original clay-size, R<sub>Car</sub>, and R<sub>Amor</sub> iron phases were observed using a scanning electron microscope (SEM, Sigma500, Key Laboratory of Surficial Geochemistry, Ministry of Education, Nanjing University) after platinum coating under the following experimental conditions: acceleration voltage = 5 kV; beam acceleration current = 240 pA, imaging mode = secondary electrons mode. The Energy Disperse Spectroscopy (Oxford, Key Laboratory of Surficial Geochemistry, Ministry of Education, Nanjing University) analysis of the residue phases before and after the addition of SRB after the aluminum coating has been performed to characterize the distribution of C and Fe elements qualitatively.

## 3. Results

### 3.1. Mineral composition

#### 3.1.1. XRD analysis

To comprehend the differences in mineral phases during the sequential chemical extracting process, the clay-sized fractions characterized by XRD were examined (Fig. S1). Kaolinite and illite are primarily minerals in the clay-size fractions of weathering deposit samples. The diffraction peaks of Fe and Mn phase minerals and hydroxyapatite were unrecognized. The characteristic peaks of Fe—Mn (hydroxide) oxide (e.g., todorokite, lepidocrocite, goethite, hematite) are likely covered by clay minerals or the crystallinity of these phases were very low, or these minerals occurred in dispersed phases (Shi et al., 1995).

#### 3.1.2. Raman analysis

Raman spectroscopy was employed to analyze the functional groups of extracted mineral phases, especially R<sub>Car</sub> and R<sub>Amor</sub> Fe phases, during chemical extraction and SRB extraction processes (Fig. 4, Fig. S2–3, Table S3).

The shapes and intensity of the absorption peak for clay-size, R<sub>Car</sub>, and R<sub>Amor</sub> Fe phases were similar. The spectra of samples measured in this study (Fig. 4; Fig. S2) before the introduction of SRB were aligned with the spectra of the hematite present in the literature (Faria et al., 1997), while following the addition of SRB, the peaks were assigned to the spectrum of goethite. For instance, ZK01, the well-established hematite bands (Faria et al., 1997) before the introduction of SRB were visible at 225 ± 5 cm<sup>-1</sup>, 291 ± 5 cm<sup>-1</sup>, 410 ± 5 cm<sup>-1</sup>, and 1320 ± 5 cm<sup>-1</sup> in the R<sub>Car</sub> and R<sub>Amor</sub> Fe phases. After the introduction of SRB, the Raman spectrum of the samples exhibited a pronounced change. For sample ZK01, peaks at 392, 677, and 1305 cm<sup>-1</sup> were seen in the spectrum of the R<sub>Car</sub> phase, corresponding to the reported spectra of goethite (392, 677 cm<sup>-1</sup>) (e.g., Oh et al., 1998). Peaks at 395, 476, and 684 cm<sup>-1</sup> were observed in the spectrum of the R<sub>Amor</sub> Fe phase, which is aligned with the reported spectra of goethite (395, 479, and 684 cm<sup>-1</sup>) (e.g., Oh et al., 1998). The peaks of the other three samples were in Fig. 4. Some peaks (e.g., 225, 291, 410, 609 cm<sup>-1</sup>) after introducing the SRB aligned with the reported spectra of hematite were visible in the R<sub>Car</sub> and R<sub>Amor</sub> Fe phases in the four samples.

#### 3.1.3. ATR-FTIR analysis

ATR-FTIR was utilized to analyze the differences in functional groups during chemical extraction and SRB-extracting experiments. The standard spectra of illite (A U.S. Geological Survey, USGS, <https://www.sciencebase.gov/catalog/>) and the residue phases before and after the addition of SRB were shown in Fig. S4 and S5. The intensity and position of peaks at 780 and 560 cm<sup>-1</sup> changed.

#### 3.1.4. DRS analysis

DRS (Diffuse reflectance spectroscopy) (Fig. S6) was used to analyze Fe oxide phases before and after the introduction of the SRB for all four samples. Regardless of whether there is an introduction of the SRB, the first-derivative spectra for R<sub>Car</sub> and R<sub>Amor</sub> iron phases revealed two bands at 575 and 436 cm<sup>-1</sup>, corresponding to hematite and goethite, respectively (Balsam et al., 2014; Ghafarpour et al., 2021; Lin et al., 2021).

#### 3.1.5. SEM and EDS analysis

SEM was used to analyze the species of Fe-minerals in the four samples. The SEM images (Fig. S7) for sample ZK81 illustrated that some needle-like minerals suspected to be goethite were observed in the clay-size and R<sub>Car</sub> phases prior to the addition of SRB, and less observed after the addition of SRB. A small amount of needle-like mineral could be observed in the R<sub>Amor</sub> Fe phase in the two reactors. The needle-like minerals were coated on the clay minerals, as well as grain size of about 2 μm long. The EDS mapping (Fig. S8) revealed decisive signals of C and Fe in the four residue phases after the introduction of SRB.

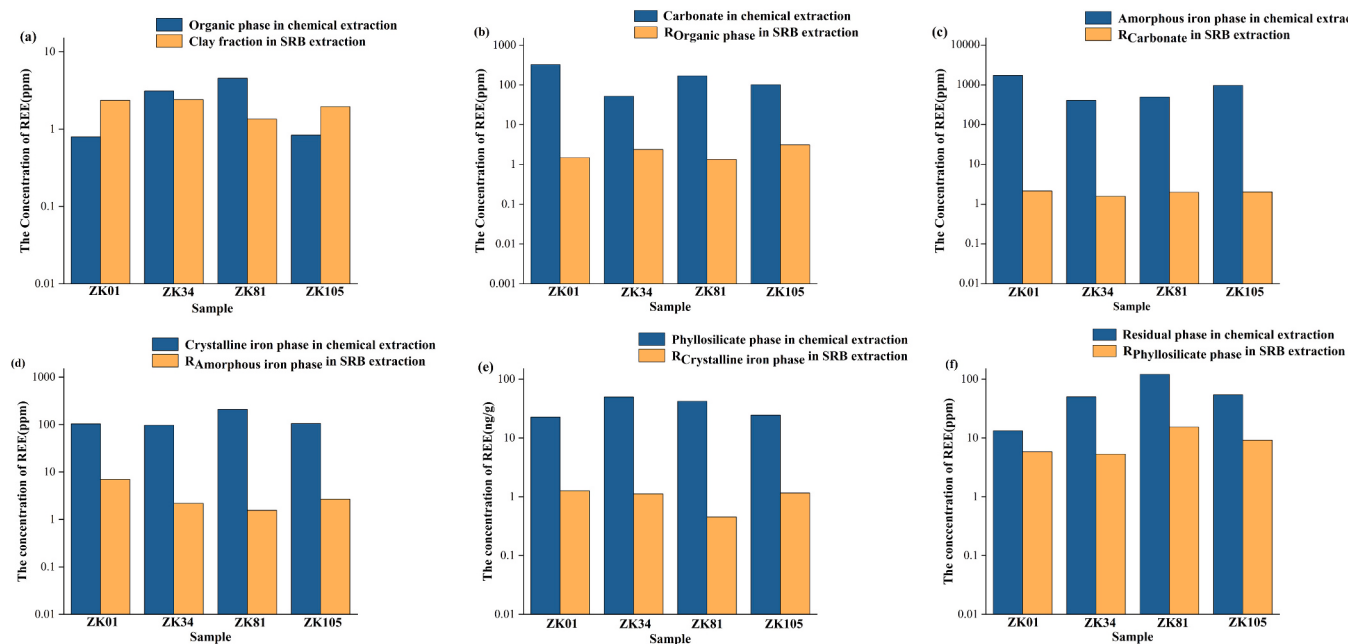


**Fig. 1.** Changes in REY concentration in clay-size fractions before and after SRB reaction. (a) the level of REY in organic phase before the SRB reaction and clay-size fractions after the reaction of SRB, (b) the level of REY in carbonate phase before the SRB reaction and R<sub>Org</sub> phase after the reaction of SRB, (c) the level of REY in amorphous iron phase before the SRB reaction and R<sub>Car</sub> phase after the reaction of SRB, (d) the level of REY in crystalline iron phase before the SRB reaction and R<sub>Amor Fe</sub> phase after the reaction of SRB, (e) the level of REY in phyllosilicate phase before the SRB reaction and R<sub>Cry Fe</sub> phase after the reaction of SRB, and (f) the level of REY in residue phase before and after the reaction of SRB.

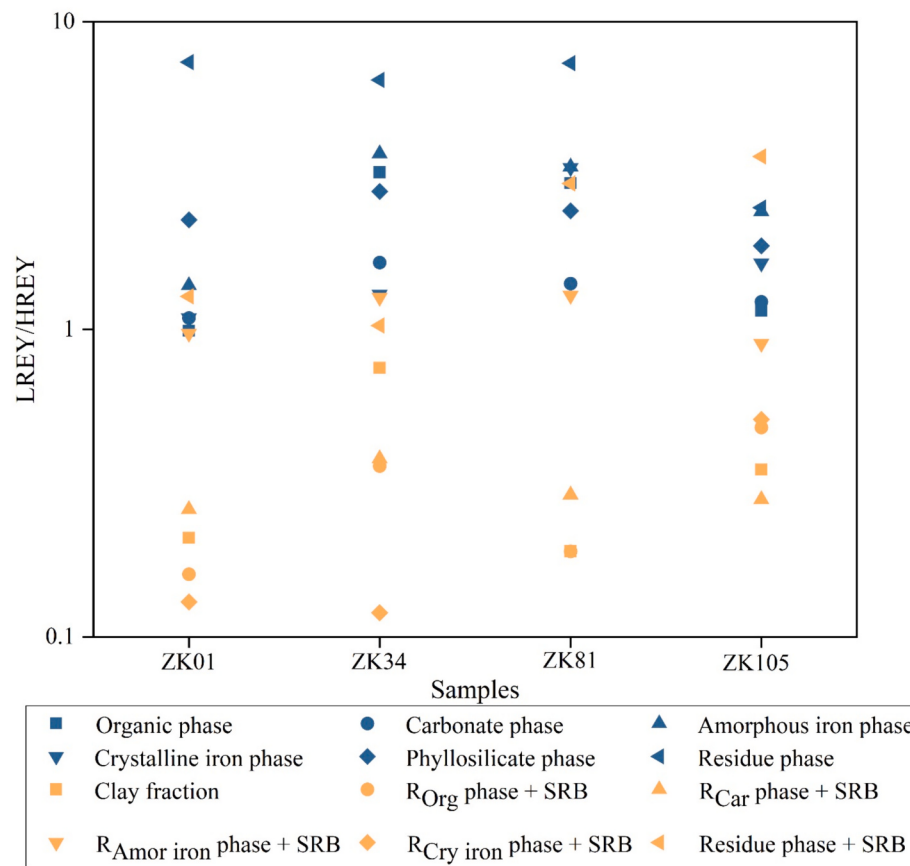


**Fig. 2.** The LREY/HREY ratios in different phases before and after the addition of SRB.

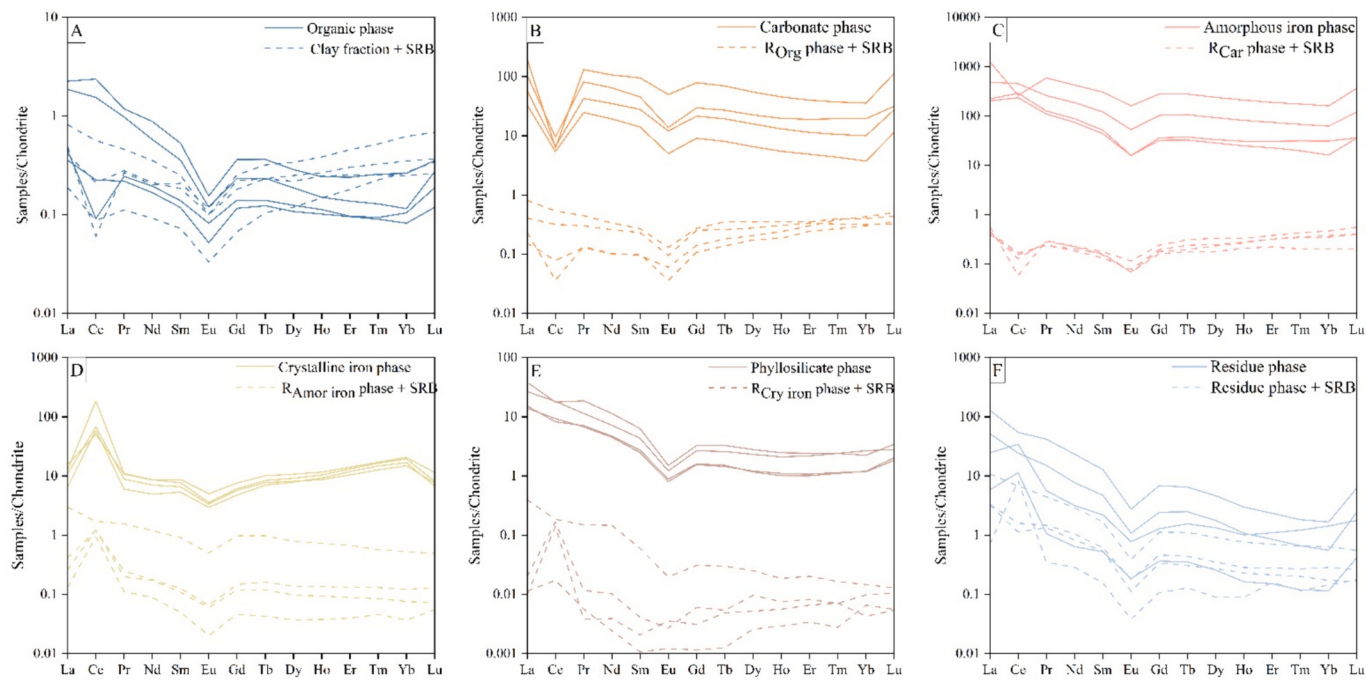


**Fig. 3.** Chondrite-normalized patterns for different phases of samples ZK01, ZK34, ZK81, and ZK105, respectively, before and after the reaction with SRB. The  $R_{Org}$  phase, after organic phase removal;  $R_{Car}$  phase, after organic and carbonate phases removal;  $R_{Amor}$  phase, after organic, carbonate, and amorphous iron phases removal;  $R_{Cry}$  phase, after organic, carbonate, amorphous iron, and crystalline Fe phases removal; Residue phase, after organic, carbonate, amorphous iron, crystalline Fe, and phyllosilicate phases removal.

### 3.2. REYs concentrations

The REY elemental concentrations of the solution in the sequential chemical extraction ( $F_A$ ) experiments and bio-extracting ( $F_B$ ) experiments are shown in Fig. 1–2, and the detailed data are documented in Tables S1 and S2. To better compare the REY concentrations among clay-size mineral phases, we simplify the clay mineral phases after introducing SRB to the most easily damaged mineral phase. For instance, we define the carbonate in the  $R_{Org}$  phase as the carbonate phase.

Before the introduction of SRB, the organic (0.79–4.54 ppm), phyllosilicate (22.56–49.61 ppm), and residue (13.22–120.25 ppm) phases have low  $\sum$ REY contents; therefore, we focus here on the remaining three fractions (i.e., the amorphous Fe phase, the carbonate phase, and crystalline Fe phase). The  $\sum$ REY levels of carbonate were 51.92–323.83 ppm (Fig. 1). Amorphous Fe–Mn ( $Fe_{ox1}$ ) isolated from the solution of sequential chemical extraction contained 1237–2355 ppm Fe, 392–1715 ppm Mn, and Mn/Fe ratios of 0.26–0.73 (Table S1). Given that Mn and Fe occur in different phases rather than a single phase (Liao et al., 2019, 2022; Kim et al., 2022), there are more amorphous Fe (oxyhydr)oxide minerals (e.g., ferrihydrite and lepidocrocite) compared to Mn minerals (e.g., vernadite, birnessite, and todorokite). The  $\sum$ REY contents vary from 408 to 1725 ppm, much higher than those from the solution of the crystalline iron phase. Crystalline Fe ( $Fe_{ox2}$ ) extracted in organic, carbonate, and amorphous iron free fractions had a concentration of Fe = 45,565–79,000 ppm. The  $Fe_{Feox2}/Fe_{Feox1}$  ratios are 29.28–45.12. The  $\sum$ REY contents vary from 96.77 to 208.3 ppm and are much lower than those from  $Fe_{Feox1}$  (Fig. 1, Table S1).

Compared to the abiotic control, the residue,  $R_{Amor}$  Fe and  $R_{Org}$  phases are the primary reservoirs for REY in the presence of SRB. The  $\sum$ REY levels in the  $R_{Org}$  phase were 1.33–3.11 ppm (Fig. 1). The Fe levels in the  $R_{Amor}$  iron phase were 82.87–247.71 ppm, higher than that in the  $R_{Car}$  phase (61.65–76.26 ppm). The  $Fe_{RAmor}/Fe_{RCar}$  ratios are 1.34–3.55 (Table S2). The  $\sum$ REY contents vary from 1.56 to 6.97 ppm and are higher than those in the  $Fe_{RCar}$  phase. Residual iron ( $Fe_R$ ) in the  $F_B$  is predominantly kaolinite and illite, with  $\sum$ REY contents of

5.3–15.35 ppm (Fig. 1, Table S2). The  $\sum$ REY contents in the residue phase in  $F_B$  accounted for 28.97%–69.67%, much higher than that (0.6%–11.55%) in  $F_A$ .

### 3.3. Incongruent release of REY

The LREY/HREY ratios and chondrite-normalized REE patterns for different mineral phases in the sequential chemical extraction ( $F_A$ ) experiments and bio-extracting ( $F_B$ ) experiments are shown in Fig. 2–3, and the detailed data are documented in Tables S1 and S2.

Before the introduction of SRB, the LREY/HREY ratios are 1.34–5.92 (Fig. 2), demonstrating the higher  $\sum$ LREY contents. Compared to the abiotic control, the LREY/HREY ratios are 0.2–1.11 after the addition of SRB (Fig. 2), slightly lower than that before the introduction of SRB. Each mineral phase has a lower ratio than the corresponding mineral phase in bio-extracting experiments, indicating the release of HREY increases in the presence of SRB.

The chondrite-normalized REY patterns for different mineral phases are shown in Fig. 3. The chondrite-normalized REY patterns for clay fraction in  $F_B$  show a notable upward trend compared to the organic phase in  $F_A$ , indicating an enrichment in HREYs of the solution. Compared with carbonate and amorphous iron phases' chondrite-normalized REY patterns, the patterns of  $R_{Org}$  and  $R_{Car}$  phases in  $F_B$  show a slightly upward trend in HREYs. The chondrite-normalized REY patterns for  $R_{Amor}$  and  $R_{Cry}$  phases exhibit inconsistent trends in HREYs, containing upward and downward trends. Both the chondrite-normalized REY patterns for the residue phases in  $F_A$  and  $F_B$  show downward trends, but the patterns of  $F_B$  are much lower than those in  $F_A$ , indicating a loss of HREYs after the introduction of SRB.

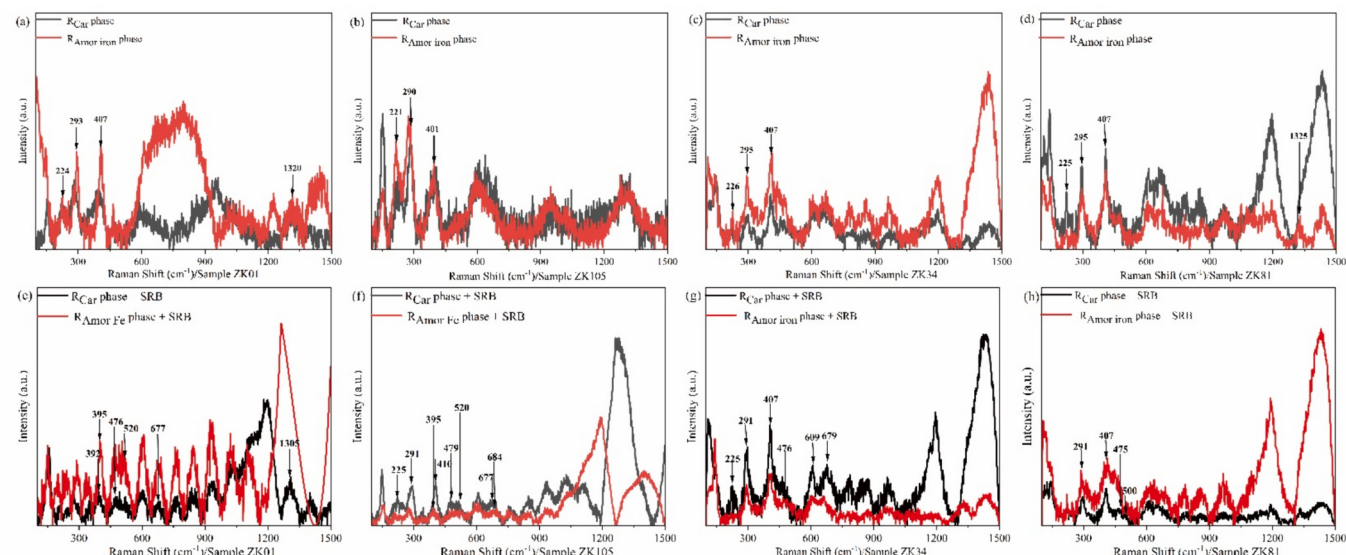


**Fig. 4.** Raman spectra for R<sub>Car</sub> and R<sub>Amor</sub> iron phases before and after reaction with SRB.

#### 4. Discussion

##### 4.1. REY in the clay-sized fraction: Predominated by $Fe_{ox1}$ and subordinated by $Fe_{ox2}$ and carbonate

The highest extraction content is observed in the amorphous Fe phase (average = 66.41%), followed by the crystalline Fe phase (average = 17.43%) and carbonate (average = 11.75%) (Fig. S9). The ATR-FTIR spectrum of different phases prior to the addition of SRB (Fig. S4) has close transmittance overlap at 400–4000  $\text{cm}^{-1}$ , suggesting that the chemical extraction process has a limited effect on functional groups. Goethite and hematite were the main Fe-minerals in this study, verified by the Raman analysis and SEM images (Fig. 4; Figs. S2, S7), demonstrating that sequential chemical extracting had little influence on the species of Fe-minerals. Therefore, the adsorption ability is the primary reason for different contents in different phases.

The concentration of REY in the amorphous Fe–Mn phase accounted for 48%–79% (Fig. S9). The  $\sum$ REY contents varied from 408 to 1725 ppm, much higher than that extracted from the solution of the crystalline iron phase. Previous studies have identified that amorphous Fe (oxyhydr)oxides with large surface areas and abundant surficial active sites incorporate more REY than amorphous Mn minerals (Jiang et al., 2011; He et al., 2023). Given that the ionic radii of  $Fe^{3+}$  and  $Mn^{4+}$  differ from those of the REY $^{3+}$ , isomorphous substitution is unlikely (Liu et al., 2023). Thus, REYs are likely adsorbed by Fe–Mn (hydr)oxides via coprecipitation or complexation under specific conditions (Bolanz et al., 2018; Li et al., 2019; Wu et al., 2023). The adsorption/complexation capacity of REYs onto Fe minerals is influenced by the style and ability of combination (e.g. -OH) (Schindler and Stumm, 1987; Tang and Johannesson, 2005). The amorphous Fe (oxyhydr)oxides opt to directly combine with free REY $^{3+}$  ions via hydroxyl ions (-OH) (Tamura et al., 2001; Wu et al., 2023).

The REY levels in the crystalline Fe phase were 97–208 ppm, accounting for 5%–20% (Fig. 1, Fig. S9), much lower than that in  $Fe_{ox1}$ . The LREY/HREY ratios in  $Fe_{ox2}$  are 1.09 to 3.35, indicating light REYs enrichment (Fig. 2). The  $Fe_{Feox2}/Fe_{Feox1}$  ratios are 25.28 to 45.12, suggesting a large amount of amorphous Fe ( $Fe_{ox1}$ ) were transformed into crystalline Fe ( $Fe_{ox2}$ ). This process involves an alteration in structure and a decrease in the specific surface area (Stumm and Sulzberger, 1992; Raiswell and Canfield, 2012). We speculate that the light REYs are more readily excluded from  $Fe_{ox2}$  during the  $Fe_{ox1}$  to  $Fe_{ox2}$  transformation, corresponding to an oxidation process.

The REY levels in the carbonate phase accounted for 8% to 16%,

varying from 52 to 324 ppm (Table S1, Fig. 1, Fig. S9). The LREY/HREY ratios were 1.09–1.65. The carbonate binding fraction encompasses the REYs bonded to carbonate (e.g. REY fluorocarbonate). REY ions are primarily complexed with carbonates following the dissolution of REY-bearing minerals in the carbonate phase, where the REY complexed with  $CO_3^{2-}$  and  $HCO_3^{2-}$  to form  $REECO_3^+$  and  $REEHCO_3^+$ , respectively (Pourret et al., 2007; Borst et al., 2020; Zhu et al., 2022).

The REY contents in these three phases accounted for 84–98%, and the organic phase, phyllosilicate phase, and residue phase host an average of 0.25%, 3.63%, and 6.01% of the  $\sum$ REYs relative to the 6-step total REY for four samples. As anticipated, the  $\Sigma$ REY contents of 2–4 steps account for >90% of the total REY from the sequential chemical extraction steps, suggesting that the REY in clay-sized REY-rich samples are bound to carbonate, amorphous Fe–Mn, and crystalline Fe phases.

##### 4.2. Mineral phase characteristics affect microbial extraction of REY

The REY concentrations in SRB extraction differ from the chemical extraction (Fig. 1 and Fig. S9 and Tables S1 and S2). The highest extraction content was observed in the residue phase (average = 45%), followed by the R<sub>Amor</sub> Fe phase (average = 17%) and R<sub>org</sub> phase (average = 11%), indicating that the introduction of SRB impacts the extraction rate of REY. Given that bacterial populations may selectively colonize onto preferred minerals for better survival (Sun et al., 2020), for instance, microorganisms can react with clay minerals, containing degrading, decomposing, and promoting the formation of other minerals and influencing their composition (Biswas et al., 2017a; Biswas et al., 2017b), above-discussion is corresponding to the results—the concentration of REYs does not decrease with the increase of sequential chemical extraction steps.

The concentration of REY in the residue phase following the introduction of SRB accounted for 29 to 70% and varied from 5.8 to 15.35 ppm (Fig. 1, Fig. S9), containing the highest level of REY among the mineral phases. Compared to the abiotic experiments, the addition of SRB resulted in a higher proportion of the residue phase. However, the residual fractions are mainly kaolinite and illite, which have weaker reducibility than iron minerals. Actually, there were additional mechanisms of Fe (III) bioreduction for clay minerals. One possibility is that certain illite layers may be of variable charge and thus bioreducible (Seabaugh et al., 2006). Another possibility is electrostatic interaction (Zhang et al., 2012). In addition, in the presence of organic ligands, Fe (II) in illite is susceptible to microbial oxidation (Weber et al., 2006; Melton et al., 2014; Bryce et al., 2018; Dong et al., 2023). The presence

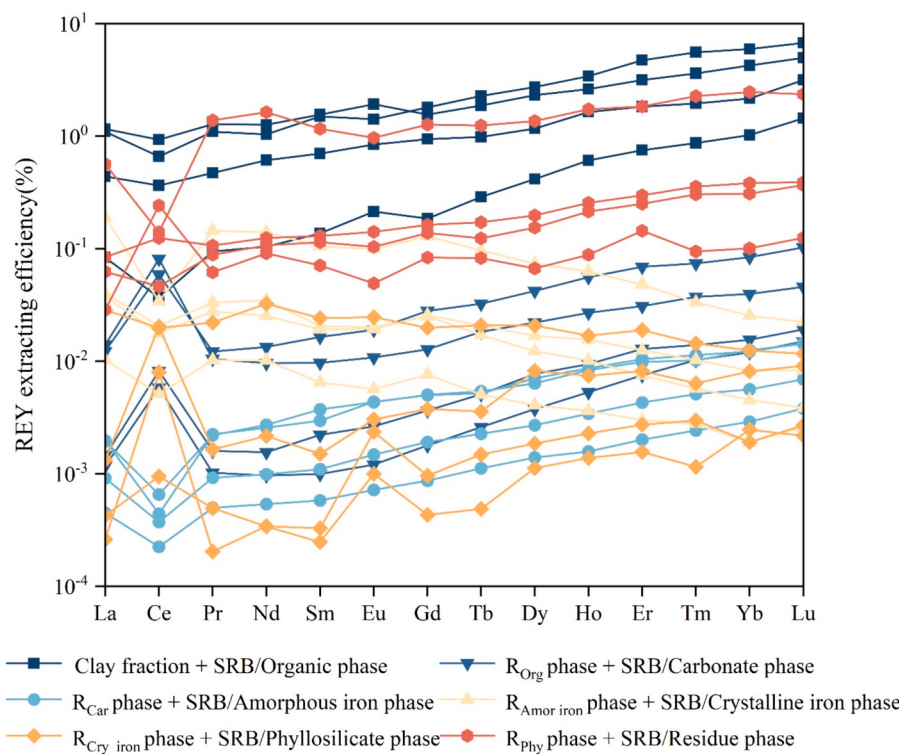


**Fig. 5.** Percentages of REY extraction from the REY-rich sample. The data are defined as the amount of dissolved concentration in chemical-extracting experiments normalized by the corresponding abundance in SRB-extracting experiments.

of ligands can improve the oxidation of structural Fe (II) in these minerals. For instance, [Xi et al. \(2020\)](#) observed that Fe (II) could accelerate the consumption of H<sup>+</sup> and sulfate by elevating the activity of the hydrogenase, which promoted the metabolic activity of SRB. The signals of C and Fe in EDS mapping (Fig. S8) indicated that it may form C—Fe coupled materials. Therefore, we speculated that C—Fe coupled materials formed in the SRB-residue reaction system, promoting the activity of SRB in the early phase. The ATR-FTIR spectra of the residue phase for all four samples illustrated that the functional groups of illite minerals changed after the introduction of SRB, which may result in the release of REY from illite (Fig. S5).

The levels of REY in the R<sub>Amor</sub> Fe phase following the introduction of SRB are 1.56–6.97 ppm, accounting for 7–35% (Fig. 1, Fig. S9). OM alters the physicochemical properties of Fe minerals, including solubility, Fe oxidation state, surface chemical, and all possible functions of OM contribute to Fe mineral transformation ([Dong et al., 2023](#)). For instance, Fe-OM co-precipitation changes both the surface and bulk properties of the mineral, resulting in disordered mineral structures ([Sodano et al., 2017](#)). The crystalline Fe minerals were initially destroyed in the R<sub>Amor</sub> Fe phase, where the Fe<sup>3+</sup> was transformed into Fe<sup>2+</sup>, which was verified by [Yan et al. \(2023\)](#), promoting the procession of reduction reactions. However, the REY content of the R<sub>Car</sub> phase was only 1.58–2.14 ppm, accounting for 9–11% (Fig. 1, Fig. S9). The most easily damaged phase in this phase was amorphous Fe minerals with poor crystallinity, which is more conducive to promoting the redox reaction between SRB and minerals. Therefore, we compared the Raman, DRS, and SEM images before and after the addition of SRB in these two phases. The DRS and SEM investigations (Figs. S6 and S7) illustrated that the four REY-rich samples had goethite and hematite in the R<sub>Car</sub> and R<sub>Amor</sub> Fe phases prior to the addition of SRB, and less observed in SEM images after the addition of SRB. The Raman spectra of the R<sub>Car</sub> and R<sub>Amor</sub> Fe phases (Fig. 4) demonstrated a new peak around 510 cm<sup>-1</sup> observed in the R<sub>Amor</sub> Fe phase, indicating that the structure and properties of Fe minerals in the R<sub>Amor</sub> Fe phase may have changed. In addition, [Yan et al. \(2023\)](#) observed that amorphous iron oxides (Fe<sub>OX</sub>) and

crystallized iron oxides (Fe<sub>CBD</sub>) reacted with SRB, forming secondary iron-bearing minerals. Hence, we hypothesize that after the addition of SRB, a large amount of amorphous iron minerals are consumed, producing Fe-OM and secondary iron-bearing minerals, resulting in an offset of the iron mineral structure and redistribution of REY, which shows the inconsistent dissolution of REY in the two iron-bearing phases and lower REY concentration than the residue phase.

The concentration of REY in the R<sub>Org</sub> phase following the introduction of SRB accounted for 6–16%, with values of 1.33–3.11 ppm (Fig. 1; Fig. S9). The concentration of REY in the clay fraction accounted for 6–16%, with a value of 1.34–2.35 ppm. The limited difference between the two phases may be attributed to low contents of REY in the organic phase ( $\sum$ REY = 0.79–4.54 ppm in the organic phase, and  $\sum$ REY = 51.92–323.83 ppm in the carbonate phase). In addition, ammonium in the Postgate liquid medium may influence the ion-exchangeable REY extraction ([Li et al., 2019](#); [Xiao et al., 2024](#)) in the clay fractions, R<sub>Org</sub>, R<sub>Car</sub>, and R<sub>Amor</sub> iron phases.

The REY contents in these three phases accounted for 66–83%, and the clay fraction, R<sub>Car</sub> phase, and R<sub>Cry</sub> iron phase host an average of 10.91%, 10.11%, and 5.4% of the  $\sum$ REYs relative to the 6-step total REY for four samples. The  $\Sigma$ REY contents of 2, 4, and 6 steps account for >74% of the total REY from the bio-extraction steps, indicating that the REY in clay-sized REY-rich samples is bound to the residue, R<sub>Amor</sub> Fe, and R<sub>Org</sub> phases.

As a promising mining method, microbial leaching is accompanied by fewer environmental problems and can enhance the extraction of MREY and HREY. Notably, the SRB-clay system has low extracting efficiency. Pure cultures of bacteria were applied for bio-extracting experiments in this study. However, the naturally bio-weathering mechanisms arising from complex microbial consortia may be much more complicated ([Fathollahzadeh et al., 2018](#); [Lamérand et al., 2020](#)), for instance, [Johnson \(2001\)](#) discovered that microbial consortia have enhanced bio-dissolution performances than pure cultures. If so, the REY release efficiency may be improved.

**Table 1**

Comparison of the primary REY speciation and LREE/HREE ratios between chemical extraction and bio-leaching experiments.

Samples	Type	Primary REY speciation	Treatment
Clay-sized fractions of Chahe ion-adsorption-type REE deposit	LREE-enriched	ion-exchangeable; amorphous Fe—Mn oxides; crystalline Fe—Mn oxides; layered silicate-bound fractions	Step 1 Ion-exchangeable fraction phase; Step 2 Organic-matter fraction; Step 3 Amorphous Fe—Mn oxides ( $Fe_{ox1}$ ) fraction; Step 4 Crystalline Fe—Mn oxides ( $Fe_{ox2}$ ) fraction; Step 5 Layered silicate-bound fraction; Step 6 Residue fraction
Clay-sized fractions of deep-sea sediments in Western Pacific Ocean	Moderately LREE-enriched	Amorphous Fe—Mn phase; Crystalline iron phase; Carbonate phase	Step 1 Carbonate; Step 2 Amorphous Fe—Mn ( $Fe_{ox1}$ ); Step 3 Crystalline iron ( $Fe_{ox2}$ ); Step 4 Fe-containing clay minerals ( $Fe_{HCL}$ ); Step 5 Residual Fe ( $Fe_R$ )
Soil samples (humic and clay layers) of Zudong Regolith-Hosted deposits	HREE-enriched	Exchangeable clay-adsorbed; Fe-Mn oxyhydroxide-adsorbed	Step 1 exchangeable clay-adsorbed component; Step 2 Fe—Mn oxyhydroxide-adsorbed component; Step 3 Organic matter-bound component; Step 4 strongly bound chemically adsorbed Fe—Mn oxyhydroxide component
Clay-sized fractions of Hanfang ion-adsorption-type REE deposit	LREE-enriched	Amorphous Fe—Mn phase; Crystalline iron phase; Carbonate phase	Step 1 Organic; Step 2 Carbonate; Step 3 Amorphous Fe—Mn ( $Fe_{ox1}$ ); Step 4 Crystalline iron ( $Fe_{ox2}$ ); Step 5 Phyllosilicate ( $Fe_{HCL}$ ); Step 6 Residual Fe ( $Fe_R$ )
Clay-sized fractions of Hanfang ion-adsorption-type REE deposit	LREE-enriched	Residue phase; $R_{Amor}$ iron phase; $R_{Org}$ phase	Step 1 Organic; Step 2 Organic and carbonate; Step 3 Organic, carbonate, and Amorphous Fe—Mn ( $Fe_{ox1}$ ); Step 4 Organic, carbonate, Amorphous Fe—Mn ( $Fe_{ox1}$ ), and Crystalline iron ( $Fe_{ox2}$ ); Step 5 Residual Fe ( $Fe_R$ )

Samples	LREE/HREE	Reference
Clay-sized fractions of Chahe ion-adsorption-type REE deposit	1.29–12.7 in ion-exchangeable; 5.81–390 in amorphous Fe—Mn oxides; 1.67–82 in crystalline Fe—Mn oxides; 3.75–98.7 in layered silicate-bound fractions	Xiao et al., 2024
Clay-sized fractions of deep-sea sediments in Western Pacific Ocean	1.01–1.57 in amorphous Fe—Mn phase; 0.39–1.21 in crystalline iron phase; 0.54–0.88 in carbonate phase	Liu et al., 2023
Soil samples (humic and clay layers) of Zudong Regolith-Hosted deposits	1.11 in exchangeable clay-adsorbed; 0.92 in Fe—Mn oxyhydroxide-adsorbed	Li et al., 2019
Clay-sized fractions of Hanfang ion-adsorption-type REE deposit	1.39–3.73 in amorphous Fe—Mn phase; 1.09–3.35 in crystalline iron phase; 1.09–1.65 in carbonate phase	This work
Clay-sized fractions of Hanfang ion-adsorption-type REE deposit	1.03–3.65 in residue phase; 0.9–1.29 in $R_{Amor}$ iron phase; 0.16–0.48 in $R_{Org}$ phase	This work

#### 4.3. REY fractionation patterns: Enhancement of MREY and HREY mobility

Prior studies have proposed that REY patterns in regolith are largely inherited from parent rocks (e.g., Bao and Zhao, 2008; Berger et al., 2014; Sanematsu et al., 2015). The Jiangxi Hanfang rock mass is a typical LREY-rich deposit, and sequentially extracted samples show significant light rare earth elements enrichment. Fig. 5 illustrates the extracting efficiency of REY in chemical and SRB extraction experiments. Not only do different mineral phases influence the fractionation of REY, but the SRB-mineral interaction also changes the REY fractionation patterns. The findings demonstrated that the addition of SRB was beneficial to utilizing middle and heavy rare earth elements.

To delve deeper into the difference in the release efficiency of REY, we examined the data by dividing REY into light (LREY; from La to Nd), middle (MREY; from Sm to Dy), and heavy REY (HREY; from Ho to Lu, and Y) (Zepf, 2013). Compared to the abiotic control, SRB enhanced MREY and HREY elemental mobilization (Fig. 5). The concentrations of dissolved REY should be linked to their abundance in different phases in chemical extracting experiments. To identify the fractionation of REY more clearly, the efficiency of elemental extraction was characterized as

the amount of dissolved concentration in chemical-extracting experiments normalized to the corresponding abundance in SRB-extracting experiments (Fig. 5). The  $REY_{FA}/REY_{FB}$  ratios were lowered in all phases except for the  $R_{Amor}$  Fe phase, indicating the addition of SRB had dissimilar REY patterns, facilitating the MREY and HREY release into the solution.

The stability of REY-ligand complexes could produce a REY fractionation (Goyne et al., 2010). By analogy to Kraemer et al. (2015), the depletion of LREY relative to MREY, with an upward pattern between La and Sm, observed in REY release efficiency patterns, could be attributed to the difference between the stabilities of LREY- and MREY- organic acid complexes. The depletion of LREY compared to MREY appeared in release efficiency patterns of various mineral phases (Fig. 5), but due to the low amounts of leached REY, a more plausible explanation was that the developed REY release patterns were probably the result of superimposed influences of mineral bond strength and the stability of REY-ligand complexes (Goyne et al., 2010). According to the aforementioned influences of organic acid ligands, HREYs could have more stable complexes with organic acid ligands than LREYs. Marsac et al. (2010) attributed the log K(REE) patterns with a MREY downward concavity to the fact that carboxylic functional groups have higher affinities with

MREY than LREY and HREY. Whereas lesser effects of organic acids, higher release efficiency of REY from Lu to La was found in all phases except for the  $R_{Amor\ Fe}$  phase.

Previous studies have demonstrated that portions of the released REY were re-scavenged during bio-weathering experiments (He et al., 2023). Therefore, a greater possibility for fractionation was that some REY might be removed by carboxylate, amines, and phosphates on bacterial surfaces, likely inducing REY fractionation in natural environments (Takahashi et al., 2010; Martinez et al., 2014). Carboxylate and phosphate groups can produce HREY enrichment on bacteria surfaces under specific conditions (Takahashi et al., 2005, 2010; Martinez et al., 2014). As goethite recrystallization is common in a hypoxic environment, it may be recrystallized or transformed into hematite with the release of phosphate and formation of  $LaPO_4/CePO_4$  precipitates under SRB conditions (Liang et al., 2024; Xu et al., 2019; Liu et al., 2021b), which brought on the HREYs enrichment in solution. Compared to the chondrite-normalized patterns before the introduction of SRB, patterns of clay-sized fractions,  $R_{Org}$ ,  $R_{Car}$ , and  $R_{Amor}$  iron phases after the introduction of SRB exhibited heavy REYs enrichment, corresponding to the transformation of goethite. Additionally, the biological functions of REY may cause the uptake of REY by microbes and influence the mobilization and fractionation of REY.  $Ce^{3+}$  and  $La^{3+}$  are necessary for the activity of methanol dehydrogenase, which is essential for methanol- and methane-utilizing bacteria to oxidize methanol (Chistoserdova, 2016). Moreover, He et al. (2023) observed that an amount of REY precipitated or co-precipitated on the surface of samples. Therefore, the production of Fe-OM in different phases is likely a method of re-adsorption of REY, producing the MREYs and HREYs enrichment in the solution.

The performances of chemical extraction and bio-leaching methods in affecting REY speciation and fractionation, which have been already explored by various groups, are denoted in Table 1. In the present research, sulfate-reducing bacteria are newly used for extracting REYs from clay-sized minerals, and they can act as an efficient way to increase the dissolution proportion of REYs in the residue phase. It can change the fractionation patterns to promote the release of MREYs and HREYs. Hence, it can be introduced as an environmentally friendly mining method for REY mining work.

## 5. Conclusions

In this study, bio-leaching experiments were executed to characterize how SRB affected the mobilization and fractionation of REY and made a comparison with chemical extracting experiments for REY behaviors. The most important conclusions of the findings of this work are as follows:

1. Chemical- and bio- extracting methods showed high potential to change the occurrence of REY in clay-sized mineral phases.
2. In chemical reactors, carbonate, amorphous iron, and crystalline iron phases with unique structures and complex capacities exhibited greater abilities to absorb REY, which highlights a link between structure, property, and hosting of REY.
3. In bio-reactors, the introduction of SRB can improve the dissolution efficiency of REY in the residue phase and REY was mainly bound to the residue, the  $R_{Amor\ Fe}$  phase, and the  $R_{Org}$  phase, where the interaction between iron cycling and organic matters was the primary cause. In addition, the transformation of goethite during bio-dissolution might influence the migration of REY.
4. The addition of SRB promoted the MREYs and HREYs fractionation from REY in bio-extracting experiments, relative to the chemical-extracting experiments.

Compared to the in situ leaching and chemical extracting methods, bio-leaching has more environmental and economic benefits. Bacteria widely found in nature have low costs and cause little environmental pollution, hence the bio-leaching approach has high practical

application potential for REY extraction.

## CRediT authorship contribution statement

**Simiao Li:** Writing – original draft, Visualization, Validation, Methodology, Formal analysis, Data curation, Conceptualization. **Yuntao Jing:** Writing – review & editing, Validation, Methodology, Conceptualization. **Xiangyu Zhu:** Writing – review & editing, Validation, Supervision. **Yan Liu:** Validation, Supervision, Investigation. **Hui Henry Teng:** Writing – review & editing, Validation, Supervision. **Hongxia Du:** Writing – review & editing, Validation, Methodology. **Wanfu Zhao:** Resources, Funding acquisition. **Ming Ma:** Methodology. **Junfeng Ji:** Writing – review & editing, Supervision, Resources, Methodology. **Wancang Zhao:** Writing – review & editing, Supervision, Methodology, Funding acquisition, Conceptualization.

## Declaration of competing interest

The authors declare that they have no known competing financial interests or personal relationships that could have appeared to influence the work reported in this paper.

## Data availability

The data in this research are available in Mendeley Data (doi:[10.17632/2tt48ykshm.1](https://doi.org/10.17632/2tt48ykshm.1)).

## Acknowledgements

This work was supported by the National Natural Science Foundation of China (Grants 92162216) and the Key Research and Development Project of the Ningxia Hui Autonomous Region, China (2022BEG03054). We thank Zuhua Liu, Qiaozhi Mao, Tengfei Ma, Jianru Cheng, Chao Guo, JiaJia Sun, Xianqiang Meng, Jie Cai, Zhanpeng Chen, haoxian Wang, Heju Hui, Hua Lin and Lisha Zhang for their assistance in the experiment.

## Appendix A. Supplementary data

Supplementary data to this article can be found online at <https://doi.org/10.1016/j.clay.2024.107534>.

## References

- Balsam, W., Ji, J.F., Renock, D., Deaton, B.C., Williams, E., 2014. Determining hematite content from NUV/Vis/NIR spectra: Limits of detection. *Am. Mineral.* 99 (11–12), 2280–2291. <https://doi.org/10.2138/am-2014-4878>.
- Bao, Z., Zhao, Z., 2008. Geochemistry of mineralization with exchangeable REY in the weathering crusts of granitic rocks in South China. *Ore Geol. Rev.* 33 (3–4), 519–535. <https://doi.org/10.1016/j.oregeorev.2007.03.005>.
- Berger, A., Janots, E., Gnos, E., Frei, R., Bernier, F., 2014. Rare earth element mineralogy and geochemistry in a laterite profile from Madagascar. *Appl. Geochem.* 41, 218–228. <https://doi.org/10.1016/j.apgeochem.2013.12.013>.
- Biswas, B., Chakraborty, A., Sarkar, B., Naidu, R., 2017a. Structural changes in smectite due to interaction with a biosurfactant-producing bacterium *Pseudoxanthomonas kaohsiungensis*. *Appl. Clay Sci.* 136, 51–57. <https://doi.org/10.1016/j.clay.2016.11.008>.
- Biswas, B., Sarkar, B., Naidu, R., 2017b. Bacterial mineralization of phenanthrene on thermally activated palygorskite: a  $^{14}C$  radiotracer study. *Sci. Total Environ.* 579, 709–717. <https://doi.org/10.1016/j.scitotenv.2016.11.037>.
- Bolanz, R.M., Kiefer, S., Goettlicher, J., Steininger, R., 2018. Hematite ( $\alpha$ -Fe $2$ O $3$ ) - a potential Ce $^{4+}$  carrier in red mud. *Sci. Total Environ.* 622, 849–860. <https://doi.org/10.1016/j.scitotenv.2017.12.043>.
- Borst, A.M., Smith, M.P., Finch, A.A., Estrade, G., Villanova-de-Benavent, C., Nason, P., Marquis, E., Horsburgh, N.J., Goodenough, K.M., Xu, C., Kynicky, J., Geraki, K., 2020. Adsorption of rare earth elements in regolith-hosted clay deposits. *Nature Communications* 11 (1). <https://doi.org/10.1038/s41467-020-17801-5>. 4386.
- Bryce, C., Blackwell, N., Schmidt, C., Otte, J., Huang, Y.-M., Kleindienst, S., Tomaszewski, E., Schad, M., Warter, V., Peng, C., Byrne, J.M., Kappler, A., 2018. Microbial anaerobic Fe (II) oxidation - Ecology, mechanisms and environmental implications. *Environ. Microbiol.* 20 (10), 3462–3483. <https://doi.org/10.1111/1462-2920.14328>.

- Chistoserdova, L., 2016. Lanthanides: New life metals? *World J. Microbiol. Biotechnol.* 32 (8), 138. <https://doi.org/10.1007/s11274-016-2088-2>.
- Dong, H., Zeng, Q., Sheng, Y., Chen, C., Yu, G., Kappler, A., 2023. Coupled iron cycling and organic matter transformation across redox interfaces. *Nat. Rev. Earth Environ.* <https://doi.org/10.1038/s43017-023-00470-5>.
- Faria, D.L.A., Venancio, Silva S., Oliveira, M.T., 1997. Roman Microspectroscopy of some Iron Oxides and Oxyhydroxides. *Raman Spectroscopy*. 28, 873–878. [https://doi.org/10.1002/\(SICI\)1097-4555\(199711\)28:11<873::AID-JRS177>3.0.CO;2-B](https://doi.org/10.1002/(SICI)1097-4555(199711)28:11<873::AID-JRS177>3.0.CO;2-B).
- Fathollahzadeh, H., Hackett, M.J., Khaleque, H.N., Eksteen, J.J., Kaksonen, A.H., Watkin, E.L.J., 2018. Better together: potential of co-culture microorganisms to enhance bioleaching of rare earth elements from monazite. *Bioresource Technol.* Rep. 3, 109–118. <https://doi.org/10.1016/j.bioteb.2018.07.003>.
- Ghafarpour, A., Khormali, F., Balsam, W., Forman, S.L., Cheng, L., Song, Y., 2021. The formation of iron oxides and magnetic enhancement mechanisms in northern Iranian loess-paleosol sequences: evidence from diffuse reflectance spectrophotometry and temperature dependence of magnetic susceptibility. *Quat. Int.* 589, 68–82. <https://doi.org/10.1016/j.quaint.2021.02.019>.
- Goyne, K.W., Brantley, S.L., Chorover, J., 2010. Rare earth element release from phosphate minerals in the presence of organic acids. *Chem. Geol.* 278 (1–2), 1–14. <https://doi.org/10.1016/j.chemgeo.2010.03.011>.
- Gu, T., Jia, R., Unsal, T., Xu, D., 2019. Toward a better understanding of microbiologically influenced corrosion caused by sulfate reducing bacteria. *J. Mater. Sci. Technol.* 35 (4), 631–636. <https://doi.org/10.1016/j.jmst.2018.10.026>.
- He, Y., Ma, L., Li, X., Wang, H., Liang, X., Zhu, J., He, H., 2023. Mobilization and fractionation of rare earth elements during experimental bio-weathering of granites. *Geochim. Cosmochim. Acta* 343, 384–395. <https://doi.org/10.1016/j.gca.2022.12.027>.
- Hasseinzadeh, G., Sajjadi, S.M., Mostafa, L., Yousefi, A., Vafaei, R.H., Zinatloo-Ajabshir, S., 2023. Synthesis of novel direct Z-scheme heterojunction photocatalyst from  $\text{WO}_3$  nanoplates and  $\text{SrTiO}_3$  nanoparticles with abundant oxygen vacancies. *Surfaces Interfaces* 42. <https://doi.org/10.1016/j.surfin.2023.103349>.
- Huang, J., Tan, W., Liang, X.L., He, H.P., Ma, L.Y., Bao, Z.W., Zhu, J.X., 2021. REE fractionation controlled by REE speciation during formation of the Renju regolith-hosted REE deposits in Guangdong Province, South China. *Ore Geology Reviews* 134. <https://doi.org/10.1016/j.oregeorev.2021.104172>.
- Ji, J.F., Chen, J., Lu, H.Y., 1999. Origin of illite in the loess from the Luochuan area, Loess Plateau, Central China. *Clay Minerals* 34 (4), 525–532. <https://doi.org/10.1180/00985599546398>.
- Ji, J.F., Balsam, W., Chen, J., Liu, L.W., 2002. Rapid and quantitative measurement of hematite and goethite in the Chinese loess-paleosol sequence by diffuse reflectance spectroscopy. *Clays Clay Miner.* 50 (2), 208–216. <https://doi.org/10.1346/00986002760832801>.
- Jiang, X., Lin, X., Yao, D., Guo, W., 2011. Enrichment mechanisms of rare earth elements in marine hydrogenic ferromanganese crusts. *Sci. China-Earth Sci.* 54 (2), 197–203. <https://doi.org/10.1007/s11430-010-4070-4>.
- Johnson, D.B., 2001. Importance of microbial ecology in the development of new mineral technologies. *Hydrometallurgy* 59 (2–3), 147–157. [https://doi.org/10.1016/s0304-386x\(00\)00183-3](https://doi.org/10.1016/s0304-386x(00)00183-3).
- Kim, M.G., Hyeyoung, K., Yoo, C.M., 2022. Distribution of rare earth elements and yttrium in sediments from the clarion-clipperton fracture zone, Northeastern Pacific Ocean. *Geochem. Geophys. Geosyst.* 23 (7) <https://doi.org/10.1029/2022gc010454> e2022GC010454.
- Ko, M.-S., Park, H.-S., Lee, J.-U., 2017. Influence of indigenous bacteria stimulation on arsenic immobilization in field study. *Catena* 148, 46–51. <https://doi.org/10.1016/j.catena.2016.08.022>.
- Kraemer, D., Kopf, S., Bau, M., 2015. Oxidative mobilization of cerium and uranium and enhanced release of "immobile" high field strength elements from igneous rocks in the presence of the biogenic siderophore desferrioxamine B. *Geochim. Cosmochim. Acta* 165, 263–279. <https://doi.org/10.1016/j.gca.2015.05.046>.
- Kumar, M., Nandi, M., Pakshirajan, K., 2021. Recent advances in heavy metal recovery from wastewater by biogenic sulfide precipitation. *J. Environ. Manage.* 278 <https://doi.org/10.1016/j.jenvman.2020.111555>.
- Lamérand, C., Shirokova, L.S., Benzeith, P., Rols, J.-L., Pokrovsky, O.S., 2020. Olivine dissolution and hydrous Mg carbonate and silicate precipitation in the presence of microbial consortium of photo-autotrophic and heterotrophic bacteria. *Geochim. Cosmochim. Acta* 268, 123–141. <https://doi.org/10.1016/j.gca.2019.09.040>.
- Li, M.Y.H., Zhou, M.-F., 2020. The role of clay minerals in formation of the regolith-hosted heavy rare earth element deposits. *Am. Mineral.* 105 (1), 92–108. <https://doi.org/10.2138/am-2020-7061>.
- Li, Y.H.M., Zhao, W.W., Zhou, M.-F., 2017. Nature of parent rocks, mineralization styles and ore genesis of regolith hosted REE deposits in South China: an integrated genetic model. *J. Asian Earth Sci.* 148, 65–95. <https://doi.org/10.1016/j.jseas.2017.08.004>.
- Li, M.Y.H., Zhou, M.F., Williams-Jones, A.E., 2019. The Genesis of Regolith-Hosted Heavy rare Earth Element deposits: Insights from the World-Class Zudong Deposit in Jiangxi Province, South China. *Econ. Geol.* 3 <https://doi.org/10.5382/econgeo.4642>.
- Li, J., Zhao, W., Du, H., Guan, Y., Ma, M., Rennenberg, H., 2022. The symbiotic system of sulfate-reducing bacteria and clay-sized fraction of purplish soil strengthens cadmium fixation through iron-bearing minerals. *Sci. Total Environ.* 820 <https://doi.org/10.1016/j.scitotenv.2022.153253>.
- Li, M., Yao, J., Wang, Y., Sunahara, G., Duran, R., Liu, J., Liu, B., Liu, H., Ma, B., Li, H., Pang, W., Cao, Y., 2024. Contrasting response strategies of sulfate-reducing bacteria in a microbial consortium to  $\text{As}^{3+}$  stress under anaerobic and aerobic environments. *J. Hazard. Mater.* 465 <https://doi.org/10.1016/j.jhazmat.2023.133052>.
- Liang, Y., Sun, X., Li, D., Peacock, C.L., Fu, Y., 2024. Effects of phosphate on REY adsorption by goethite: Insights into REY enrichment and release in marine iron oxyhydroxides during early diagenesis. *Chem. Geol.* 649 <https://doi.org/10.1016/j.chemgeo.2024.121966>.
- Liao, J., Sun, X., Wu, Z., Sa, R., Guan, Y., Lu, Y., Li, D., Liu, Y., Deng, Y., Pan, Y., 2019. Fe-Mn (oxyhydr)oxides as an indicator of REY enrichment in deep-sea sediments from the central North Pacific. *Ore Geol. Rev.* 112 <https://doi.org/10.1016/j.oregeorev.2019.103044>.
- Liao, J., Chen, J., Sun, X., Wu, Z., Deng, Y., Shi, X., Wang, Y., Chen, Y., Koschinsky, A., 2022. Quantifying the controlling mineral phases of rare-earth elements in deep-sea pelagic sediments. *Chem. Geol.* 595 <https://doi.org/10.1016/j.chemgeo.2022.120792>.
- Lin, Z., Natoli, J.M., Picuri, J.C., Shaw, S.E., Bowyer, W.J., 2021. Replication of the conversion of goethite to hematite to make pigments in both furnace and campfire. *J. Archaeol. Sci.-Rep.* 39 <https://doi.org/10.1016/j.jasrep.2021.103134>.
- Liu, W.-S., Guo, M.-N., Liu, C., Yuan, M., Chen, X.-T., Huot, H., Zhao, C.-M., Tang, Y.-T., Morel, J.-L., Qiu, R.-L., 2019. Water, sediment and agricultural soil contamination from an ion-adsorption rare earth mining area. *Chemosphere* 216, 75–83. <https://doi.org/10.1016/j.chemosphere.2018.10.109>.
- Liu, J., Liu, W., Zhang, Y., Chen, C., Wu, W., Zhang, T.C., 2021a. Microbial communities in rare earth mining soil after in-situ leaching mining. *Sci. Total Environ.* 755 <https://doi.org/10.1016/j.scitotenv.2020.142521>.
- Liu, J., Zhu, R., Ma, L., Fu, H., Lin, X., Parker, S.C., Molinari, M., 2021b. Adsorption of phosphate and cadmium on iron (oxyhydr)oxides: a comparative study on ferrihydrite, goethite, and hematite. *Geoderma* 383. <https://doi.org/10.1016/j.geoderma.2020.114799>.
- Liu, Y., Jing, Y., Zhao, W., 2023. Distribution of rare earth elements and implication for Ce anomalies in the clay-sized minerals of deep-sea sediment, Western Pacific Ocean. *Applied Clay Science* 235. <https://doi.org/10.1016/j.clay.2023.106876>.
- Lu, W.Y., Zhao, W.C., Balsam, W., Lu, H., Liu, P., Lu, Z.L., Ji, J.F., 2017. Iron Mineralogy and Speciation in Clay-Sized Fractions of Chinese Desert Sediments. *J. Geophys. Res.-Atmos.* 122 (24), 13458–13471. <https://doi.org/10.1002/2017jd027733>.
- Marsac, R., Davranche, M., Gruaud, G., Dia, A., 2010. Metal loading effect on rare earth element binding to humic acid: Experimental and modelling evidence. *Geochim. Cosmochim. Acta* 74 (6), 1749–1761. <https://doi.org/10.1016/j.gca.2009.12.006>.
- Martinez, R.E., Pourret, O., Takahashi, Y., 2014. Modeling of rare earth element sorption to the Gram positive *Bacillus subtilis* bacteria surface. *J. Colloid Interface Sci.* 413, 106–111. <https://doi.org/10.1016/j.jcis.2013.09.037>.
- Mehra, O., Jackson, M., 1958. Iron oxide removal from soils and clays by a dithionitecitrate system buffered with sodium bicarbonate. *Clays Clay Miner.* 7 (1), 317–327. <https://doi.org/10.1346/cmm.1958.0070122>.
- Melton, E.D., Swanner, E.D., Behrens, S., Schmidt, C., Kappler, A., 2014. The interplay of microbially mediated and abiotic reactions in the biogeochemical Fe cycle. *Nat. Rev. Microbiol.* 12 (12), 797–808. <https://doi.org/10.1038/nrmicro3347>.
- Moldoveanu, G.A., Papangelakis, V.G., 2013. Recovery of rare earth elements adsorbed on clay minerals: II. Leaching with ammonium sulfate. *Hydrometallurgy* 131, 158–166. <https://doi.org/10.1016/j.hydromet.2012.10.011>.
- Moore, D.M., Reynolds, R.C., 1997. X-Ray Diffraction and the Identification and Analysis of Clay Minerals, 2nd ed. Oxford University Press, Oxford. [http://refhub.elsevier.com/S0169-1317\(23\)00063-7/rf0220](http://refhub.elsevier.com/S0169-1317(23)00063-7/rf0220).
- Oh, S.J., Cook, D.C., Townsend, H.E., 1998. Characterization of iron oxides commonly formed as corrosion products on steel. *Hyperfine Interact.* 112 (1–4), 59–65. <https://doi.org/10.1023/a:1011076308501>.
- Ou, X., Chen, Z., Chen, X., Li, X., Wang, J., Ren, T., Chen, H., Feng, L., Wang, Y., Chen, Z., Liang, M., Gao, P., 2022. Redistribution and chemical speciation of rare earth elements in an ion- adsorption rare earth tailing, Southern China. *Sci. Total Environ.* 821 <https://doi.org/10.1016/j.scitotenv.2022.153369>.
- Owusu-Fordjour, E.Y., Yang, X., 2023. Bioleaching of rare earth elements challenges and opportunities: a critical review. *Journal of Environmental. Chem. Eng.* 11 (5), 110413 <https://doi.org/10.1016/j.jece.2023.110413>.
- Postgate, J.R., Campbell, L.L., 1966. Classification of *desulfovibrio* species, the nonsporulating sulfate-reducing bacteria. *Bacteriol. Rev.* 30 (4), 732–738. <https://doi.org/10.1128/mmbr.30.4.732-738.1966>.
- Poulton, S.W., Canfield, D.E., 2005. Development of a sequential extraction procedure for iron: implications for iron partitioning in continental derived particulates. *Chem. Geol.* 214 (3–4), 209–221. <https://doi.org/10.1016/j.chemgeo.2004.09.003>.
- Pourret, O., Davranche, M., Gruaud, G., Dia, A., 2007. Competition between humic acid and carbonates for rare earth elements complexation. *J. Colloid Interface Sci.* 305 (1), 25–31. <https://doi.org/10.1016/j.jcis.2006.09.020>.
- Raiswell, R., Canfield, D.E., 2012. The iron biogeochemical cycle past and present. *Geochim. Perspectives* 1 (1), 1–220. <https://doi.org/10.7185/geochempersp.1.1>.
- Sanematsu, K., Kon, Y., Imai, A., 2015. Influence of phosphate on mobility and adsorption of REEs during weathering of granites in Thailand. *J. Asian Earth Sci.* 111, 14–30. <https://doi.org/10.1016/j.jseas.2015.05.018>.
- Schindler, P.W., Stumm, W., 1987. The surface chemistry of oxides, hydroxides, and oxides minerals. In: Stumm, W. (Ed.), *Aquatic Surface Chemistry. Chemical processes at the Particle-Water Interface*, John Wiley and Sons, New York, pp. 83–110.
- Seabaugh, J.L., Dong, H., Kukkadapu, R.K., Eberl, D.D., Morton, J.P., Kim, J., 2006. Microbial reduction of Fe (III) in the Fithian and Muloorina illites: contrasting extents and rates of bioreduction. *Clays Clay Miner.* 54 (1), 67–79. <https://doi.org/10.1346/ccmn.2006.0540109>.
- Shi, N., Ma, Z., He, W., Luo, J., 1995. Nano-solids in manganese nodules from northern part of Pacific Ocean floorNano-solids in minerals and prospects of its uses in industry. *Sci. China B* 38 (12), 1493–1500 doi.org/CNKI:SUN:JBXG.0.1995-12-010.

- Sodano, M., Lerda, C., Nistico, R., Martin, M., Magnacca, G., Celi, L., Said-Pullicino, D., 2017. Dissolved organic carbon retention by coprecipitation during the oxidation of ferrous iron. *Geoderma* 307, 19–29. <https://doi.org/10.1016/j.geoderma.2017.07.022>.
- Stumm, W., Sulzberger, B., 1992. The cycling of iron in natural environments: Considerations based on laboratory studies of heterogeneous redox processes. *Geochim. Cosmochim. Acta* 56 (8), 3233–3257. [https://doi.org/10.1016/0016-7037\(92\)90301-x](https://doi.org/10.1016/0016-7037(92)90301-x).
- Sun, Q., Liu, X., Wang, S., Lian, B., 2020. Effects of mineral substrate on ectomycorrhizal fungal colonization and bacterial community structure. *Sci. Total Environ.* 721 <https://doi.org/10.1016/j.scitotenv.2020.137663>. 137663.
- Takahashi, Y., Châtellier, X., Hattori, K.H., Kato, K., Fortin, D., 2005. Adsorption of rare earth elements onto bacterial cell walls and its implication for REE sorption onto natural microbial mats. *Chem. Geol.* 219 (1–4), 53–67. <https://doi.org/10.1016/j.chemgeo.2005.02.009>.
- Takahashi, Y., Yamamoto, M., Yamamoto, Y., Tanaka, K., 2010. EXAFS study on the cause of enrichment of heavy REEs on bacterial cell surfaces. *Geochim. Cosmochim. Acta* 74 (19), 5443–5462. <https://doi.org/10.1016/j.gca.2010.07.001>.
- Tamura, H., Mita, K., Tanaka, A., Ito, M., 2001. Mechanism of hydroxylation of metal oxide surfaces. *J. Colloid Interface Sci.* 243 (1), 202–207. <https://doi.org/10.1006/jcis.2001.7864>.
- Tang, J.W., Johannesson, K.H., 2005. Adsorption of rare earth elements onto Carrizo sand: Experimental investigations and modeling with surface complexation. *Geochim. Cosmochim. Acta* 69 (22), 5247–5261. <https://doi.org/10.1016/j.gca.2005.06.021>.
- Taunton, A.E., Welch, S.A., Banfield, J.F., 2000. Microbial controls on phosphate and lanthanide distributions during granite weathering and soil formation. *Chem. Geol.* 169 (3–4), 371–382. [https://doi.org/10.1016/s0009-2541\(00\)00215-1](https://doi.org/10.1016/s0009-2541(00)00215-1).
- Wang, G., Xu, J., Ran, L., Zhu, R., Ling, B., Liang, X., Kang, S., Wang, Y., Wei, J., Ma, L., Zhuang, Y., Zhu, J., He, H., 2023. A green and efficient technology to recover rare earth elements from weathering crusts. *Nature Sustainability* 6 (1), 81–92. <https://doi.org/10.1038/s41893-022-00989-3>.
- Weber, K.A., Achenbach, L.A., Coates, J.D., 2006. Microorganisms pumping iron: anaerobic microbial iron oxidation and reduction. *Nat. Rev. Microbiol.* 4 (10), 752–764. <https://doi.org/10.1038/nrmicro1490>.
- Wu, L., Jacobson, A.D., Hausner, M., 2008. Characterization of elemental release during microbe-granite interactions at T = 28°C. *Geochim. Cosmochim. Acta* 72 (4), 1076–1095. <https://doi.org/10.1016/j.gca.2007.11.025>.
- Wu, Z., Chen, Y., Wang, Y., Xu, Y., Lin, Z., Liang, X., Cheng, H., 2023. Review of rare earth element (REE) adsorption on and desorption from clay minerals: Application to formation and mining of ion-adsorption REE deposits. *Ore Geol. Rev.* 157 <https://doi.org/10.1016/j.oregeorev.2023.105446.105446>.
- Xi, Y., Lan, S., Li, X., Wu, Y., Yuan, X., Zhang, C., Liu, Y., Huang, Y., Quan, B., Wu, S., 2020. Bioremediation of antimony from wastewater by sulfate-reducing bacteria: effect of the coexisting ferrous ion. *Int. Biodegrad. Biodegr.* 148 <https://doi.org/10.1016/j.ibiod.2020.104912.104912>.
- Xiao, Y.-F., Chen, Y.-Y., Feng, Z.-Y., Huang, X.-W., Huang, L., Long, Z.-Q., Cui, D.-L., 2015. Leaching characteristics of ion-adsorption type rare earths ore with magnesium sulfate. *Trans. Nonferrous Met. Soc. Chin.* 25 (11), 3784–3790. [https://doi.org/10.1016/s1003-6326\(15\)64022-5](https://doi.org/10.1016/s1003-6326(15)64022-5).
- Xiao, S., Liu, Y., Zhao, W., 2024. Redox constraints on clay-sized rare earth element fractionation in weathered granite crust in the Chahe deposit, China. *Appl. Clay Sci.* 254 <https://doi.org/10.1016/j.clay.2024.107365>.
- Xu, C., Kynicky, J., Smith, M.P., Kopriva, A., Brtnicky, M., Urubek, T., Yang, Y., Zhao, Z., He, C., Song, W., 2017. Origin of heavy rare earth mineralization in South China. *Nat. Commun.* 8 <https://doi.org/10.1038/ncomms14598.14598>.
- Xu, T., Zhu, R., Shang, H., Xia, Y., Liu, X., Zhang, L., 2019. Photochemical behavior of ferrihydrite-oxalate system: Interfacial reaction mechanism and charge transfer process. *Water Res.* 159, 10–19. <https://doi.org/10.1016/j.watres.2019.04.055>.
- Yan, X., Guan, D.-X., Li, J., Song, Y., Tao, H., Zhang, X., Ma, M., Ji, J., Zhao, W., 2023. Fate of Cd during mineral transformation by sulfate-reducing bacteria in clay-size fractions from soils with high geochemical background. *J. Hazard. Mater.* 459, 132213. <https://doi.org/10.1016/j.jhazmat.2023.132213>.
- Zepf, V., 2013. Rare earth elements: What and where they are. In: *Rare Earth Elements*. Springer, Berlin Heidelberg, Berlin, Heidelberg, pp. 11–39.
- Zhang, J., Dong, H., Liu, D., Fischer, T.B., Wang, S., Huang, L., 2012. Microbial reduction of Fe (III) in illite-smectite minerals by methanogen *Methanosarcina mazei*. *Chem. Geol.* 292, 35–44. <https://doi.org/10.1016/j.chemgeo.2011.11.003>.
- Zhang, Q., Ren, F., Li, F., Chen, G., Yang, G., Wang, J., Du, K., Liu, S., Li, Z., 2020. Ammonia nitrogen sources and pollution along soil profiles in an in-situ leaching rare earth ore. *Environ. Pollut.* 267, <https://doi.org/10.1016/j.envpol.2020.115449>.
- Zhao, W., Sun, Y., Balsam, W., Zeng, L., Lu, H., Otgonbayar, K., Ji, J., 2015. Clay-sized Hf-Nd-Sr isotopic composition of Mongolian dust as a fingerprint for regional to hemispherical transport. *Geophys. Res. Lett.* 42 (13), 5661–5669. <https://doi.org/10.1002/2015gl064357>.
- Zhao, Y., Zou, X., Gao, J., Wang, C., Li, Y., Yao, Y., Zhao, W., Xu, M., 2018. Clay mineralogy and source-to-sink transport processes of Changjiang River sediments in the estuarine and inner shelf areas of the East China Sea. *J. Asian Earth Sci.* 152, 91–102. <https://doi.org/10.1016/j.jseas.2017.11.038>.
- Zhou, F., Liu, Q., Feng, J., Su, J., Liu, X., Chi, R., 2019. Role of initial moisture content on the leaching process of weathered crust elution-deposited rare earth ores. *Sep. Purif. Technol.* 217, 24–30. <https://doi.org/10.1016/j.seppur.2019.02.010>.
- Zhu, X., Zhang, B., Ma, G., Pan, Z., Hu, Z., Zhang, B., 2022. Mineralization of ion-adsorption type rare earth deposits in Western Yunnan, China. *Ore Geol. Rev.* 148 <https://doi.org/10.1016/j.oregeorev.2022.104984.104984>.
- Zinatloo-Ajabshir, S., Salavati-Niasari, M., 2016. Facile route to synthesize zirconium dioxide ( $\text{ZrO}_2$ ) nanostructures: Structural, optical and photocatalytic studies. *J. Mol. Liq.* 216, 545–551. <https://doi.org/10.1016/j.molliq.2016.01.062>.
- Zinatloo-Ajabshir, S., Salavati-Niasari, M., 2019. Preparation of magnetically retrievable  $\text{CoFe}_2\text{O}_4@\text{SiO}_2@\text{Dy}_2\text{Ce}_2\text{O}_7$  nanocomposites as novel photocatalyst for highly efficient degradation of organic contaminants. *Compos. Part B Eng.* 174 <https://doi.org/10.1016/j.compositesb.2019.106930>.
- Zinatloo-Ajabshir, S., Rakhsani, S., Mehrabadi, Z., Farsadrooh, M., Feizi-Dehnayebi, M., Rakhsani, S., Dušek, M., Eigner, V., Rtimi, S., Aminabhavi, T.M., 2024. Novel rod-like  $[\text{Cu}(\text{phen})_2(\text{OAc})]\cdot\text{PF}_6$  complex for high-performance visible-light-driven photocatalytic degradation of hazardous organic dyes: DFT approach, Hirshfeld and fingerprint plot analysis. *J. Environ. Manage.* 350 <https://doi.org/10.1016/j.jenvman.2023.119545>.